

## Two-Scale Modelling of Reactive Powder Concrete. Part II: Numerical Simulations

Arkadiusz DENISIEWICZ<sup>1)</sup>, Mieczysław KUCZMA<sup>2)</sup>

<sup>1)</sup> *University of Zielona Góra  
Division of Structural Mechanics*

Prof. Z. Szafrana 1, 65-246 Zielona Góra, Poland  
e-mail: a.denisiewicz@ib.uz.zgora.pl

<sup>2)</sup> *Poznan University of Technology  
Institute of Structural Engineering*

Piotrowo 5, 61-965 Poznań, Poland  
e-mail: mieczyslaw.kuczma@put.poznan.pl

This article is the second part of a series about two-scale modelling of reactive powder concrete (RPC). In the first part [2] a method of modelling RPC microstructure was presented, the boundary value problem of mechanics for a representative cell at the micro scale was formulated and solved. In this part we will consider a method for determining material parameters at the macro level, and describe a technique of enforcement of boundary conditions upon an RVE as well as illustrate the theoretical considerations with results of numerical simulations. In the third part of the series we will present the validation of the proposed numerical model, based on the computational simulations of full size beams made of two RPC mixtures and own laboratory testing of the beams.

**Key words:** two-scale modelling, numerical homogenization, RPC, FEM, numerical simulations.

### 1. SOLUTION TO THE BOUNDARY VALUE PROBLEM AT MICRO LEVEL

For the sake of clarity the formulation of the boundary value problem of mechanics from the first part of the series will be repeated [3]. The boundary value problem for a particular representative volume element (RVE), after the finite element discretization, can be solved by minimising the energy function with additionally imposed constraints on the unknown vector of displacements  $\mathbf{u}$ :

$$(1.1) \quad \min_{\mathbf{u}} \varphi(\mathbf{u}) = \frac{1}{2} \mathbf{u}^T \mathbf{K} \mathbf{u} - \mathbf{u}^T \mathbf{f}$$

with conditions  $\mathbf{C} \mathbf{u} - \mathbf{g} = \mathbf{0}$ ,

where  $\mathbf{K}$  is the stiffness matrix,  $\mathbf{C}$  – compatibility matrix,  $\mathbf{f}$  – vector of loads, and  $\mathbf{g}$  – vector of constraints.

This constrained minimization problem can be reduced, as shown in [1, 7], to solving a system of linear equations:

$$(1.2) \quad \tilde{\mathbf{K}}\mathbf{u} = \tilde{\mathbf{F}}$$

in which

$$(1.3) \quad \tilde{\mathbf{K}} = \sum_e [(\mathbf{C}_u^e)^T \mathbf{C}_u^e + (\mathbf{Q}_u^e)^T \mathbf{K}^e \mathbf{Q}_u^e],$$

$$(1.4) \quad \tilde{\mathbf{F}} = \sum_e [\mathbf{D}_u^e \bar{\boldsymbol{\varepsilon}} (\mathbf{C}_u^e)^T - (\mathbf{Q}_u^e)^T \mathbf{K}^e \mathbf{R}_u^e],$$

$$(1.5) \quad \mathbf{Q}_u^e = \mathbf{I} - \mathbf{R}_u^e \mathbf{C}_u^e,$$

$$(1.6) \quad \mathbf{R}_u^e = (\mathbf{C}_u^e)^T [\mathbf{C}_u^e (\mathbf{C}_u^e)^T]^{-1}.$$

The symbol  $\sum_e$  denotes the aggregation of finite elements  $e$  in micro scale. In order to enforce RVE deformations consistent with the macro deformation  $\bar{\boldsymbol{\varepsilon}}$  displacement boundary conditions of the first type were used [7, 12].

## 2. DISPLACEMENT BOUNDARY CONDITIONS

Displacement boundary conditions are imposed as linear deformation on the boundary  $\Gamma$  and they can be defined as follows:

$$(2.1) \quad \mathbf{u} \equiv \mathbf{x} \cdot \bar{\boldsymbol{\varepsilon}} \quad \forall \mathbf{x} \in \Gamma.$$

The Eq. (2.1) can also be written as

$$(2.2) \quad \mathbf{r}(\mathbf{x}) = \mathbf{0} \quad \forall \mathbf{x} \in \Gamma$$

with  $\mathbf{r}(\mathbf{x})$  being the micro fluctuation of the displacement area, which automatically satisfies the static boundary condition. The equation expressed in the form of weighted residues will take the form

$$(2.3) \quad \int_{\Gamma} \delta \mathbf{t} \cdot (\mathbf{u} - \mathbf{x} \cdot \bar{\boldsymbol{\varepsilon}}) d\Gamma = 0 \quad \forall \delta \mathbf{t}.$$

This method of writing displacement boundary conditions is very convenient when the task is solved on micro level with the method of finite elements. After the discretization of the boundary value problem, the Eq. (2.3) will lead to

a system of  $n$ -algebraic equations, where  $n$  denotes the number of degrees of freedom on the boundary  $\Gamma$  of a representative volume element.

Using (2.3) we can write the displacement boundary conditions in a matrix form

$$(2.4) \quad \mathbf{C}_u^e \mathbf{u} = \mathbf{D}_u^e \bar{\boldsymbol{\varepsilon}} = \mathbf{g}_u^e,$$

where

$$(2.5) \quad \mathbf{C}_u^e = \int_{\Gamma} \mathbf{H}_u \mathbf{N}^T \mathbf{N} d\Gamma,$$

$$(2.6) \quad \mathbf{D}_u^e = \int_{\Gamma} \mathbf{H}_u \mathbf{N}^T \mathbf{X} d\Gamma,$$

$$(2.7) \quad \mathbf{X} = \frac{1}{2} \begin{bmatrix} 2\xi & 0 & \eta \\ 0 & 2\eta & \xi \end{bmatrix}.$$

The rows of the matrix being the product  $\mathbf{H}_u \mathbf{N}^T$  can be interpreted as linearly independent functions of the distribution of admissible boundary forces, and the columns of the matrix  $\mathbf{H}_u$  can be interpreted as the values of nodal forces. Because of the fact that for displacement boundary conditions any distribution of boundary forces is permissible, we have adopted

$$\mathbf{H}_u = \text{diag} [ 1 \ 1 \ 1 \ 1 \ 1 \ 1 \ 1 \ 1 ].$$

The Eq. (2.4) enforces on RVE the deformation according to the imposed macro deformation measures  $\bar{\boldsymbol{\varepsilon}}$  and results in a zero value of the work of the permissible distributions of boundary forces on the micro fluctuations of the displacement area.

### 3. DETERMINATION OF MATERIAL PARAMETERS AT MACRO LEVEL

The macro stresses, which may be interpreted here as components of the elasticity matrices  $\bar{\mathbf{C}}$  are determined for the macro scale analysis by solving three linear systems of equations for RVE [7]

$$(3.1) \quad \begin{aligned} \delta \bar{\boldsymbol{\sigma}}^1 & \text{ for } \delta \bar{\boldsymbol{\varepsilon}} = [1, 0, 0], \\ \delta \bar{\boldsymbol{\sigma}}^2 & \text{ for } \delta \bar{\boldsymbol{\varepsilon}} = [0, 1, 0], \\ \delta \bar{\boldsymbol{\sigma}}^3 & \text{ for } \delta \bar{\boldsymbol{\varepsilon}} = [0, 0, 1], \end{aligned}$$

$$(3.2) \quad \bar{\mathbf{C}} = [ \delta \bar{\boldsymbol{\sigma}}^1 \quad \delta \bar{\boldsymbol{\sigma}}^2 \quad \delta \bar{\boldsymbol{\sigma}}^3 ], \quad \bar{\mathbf{C}} = \begin{bmatrix} \delta \bar{\sigma}_{11}^1 & \delta \bar{\sigma}_{11}^2 & \delta \bar{\sigma}_{11}^3 \\ \delta \bar{\sigma}_{22}^1 & \delta \bar{\sigma}_{22}^2 & \delta \bar{\sigma}_{22}^3 \\ \delta \bar{\sigma}_{12}^1 & \delta \bar{\sigma}_{12}^2 & \delta \bar{\sigma}_{12}^3 \end{bmatrix},$$

where

$$(3.3) \quad \bar{\boldsymbol{\sigma}} = \frac{1}{V} \sum_e (\mathbf{D}_u^e)^T \boldsymbol{\lambda}^e,$$

$$(3.4) \quad \boldsymbol{\lambda}^e = (\mathbf{R}_u^e)^T (\mathbf{F}^e - \mathbf{K}^e \mathbf{u}^e),$$

$\mathbf{u}^e = \mathbf{q}$  is the vector of nodal micro displacements of the RVE,  $\mathbf{F}^e = \mathbf{0}$  is the vector of nodal micro loads on the RVE of volume  $V$ .

Using (3.2) and (3.3) for a plane state of stress and for isotopic linearly elastic micro components, we will obtain

$$(3.5) \quad \bar{\mathbf{C}} = \begin{bmatrix} \bar{C}_{11} & \bar{C}_{12} & 0 \\ \bar{C}_{21} & \bar{C}_{22} & 0 \\ 0 & 0 & \bar{C}_{33} \end{bmatrix},$$

where  $\bar{C}_{11} = \bar{C}_{22} \neq 0$ ,  $\bar{C}_{12} = \bar{C}_{21} \neq 0$ ,  $\bar{C}_{33} \neq 0$  and assuming at a macro scale level the form of the matrix of material elasticity like for isotropy, on the basis of a numerical solution, it is possible to determine material parameters of a homogenized medium at the macro scale.

$$(3.6) \quad \begin{bmatrix} \bar{C}_{11} & \bar{C}_{12} & 0 \\ \bar{C}_{12} & \bar{C}_{22} & 0 \\ 0 & 0 & \bar{C}_{33} \end{bmatrix} = \begin{bmatrix} \frac{\bar{E}}{1-\bar{\nu}^2} & \frac{\bar{\nu}\bar{E}}{1-\bar{\nu}^2} & 0 \\ \frac{\bar{\nu}\bar{E}}{1-\bar{\nu}^2} & \frac{\bar{E}}{1-\bar{\nu}^2} & 0 \\ 0 & 0 & \bar{G} \end{bmatrix}, \quad \text{where } \bar{G} = \frac{\bar{E}}{2(1+\bar{\nu})}.$$

After solving the above system of three equations with three unknown values  $\bar{E}$ ,  $\bar{\nu}$ ,  $\bar{G}$ , we will obtain Young's modulus, Poisson's ratio and the shear modulus (Kirchhoff's modulus) respectively

$$(3.7) \quad \bar{E} = \frac{\bar{C}_{11}^2 - \bar{C}_{12}^2}{\bar{C}_{11}},$$

$$(3.8) \quad \bar{\nu} = \frac{\bar{C}_{12}}{\bar{C}_{11}},$$

$$(3.9) \quad \bar{G} = \frac{\bar{C}_{11} - \bar{C}_{12}}{2} = \bar{C}_{33}.$$

## 4. METHOD OF ENFORCING BOUNDARY CONDITIONS

In order to correctly force RVE deformations, consistent with the macro deformation  $\bar{\epsilon}$ , which has to be “located” only on the boundary  $\Gamma$ , during the aggregation of the matrix (1.3) and the vector of right-hand sides (1.4) of the system of Eqs. (1.2), we proceed according to the scheme presented below.

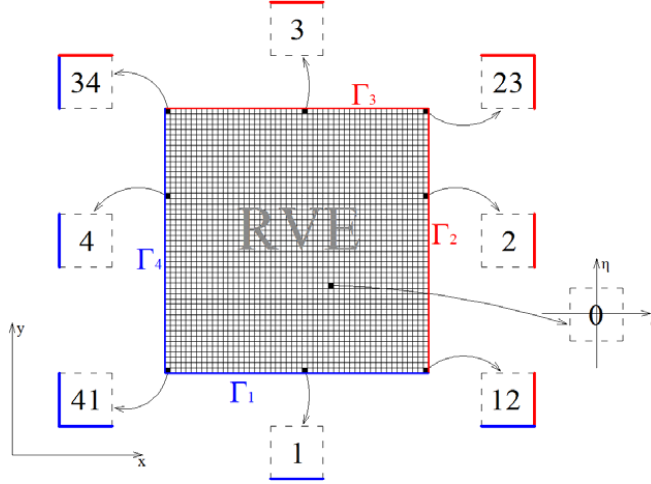


FIG. 1. A scheme of the enforcement of boundary conditions upon the RVE.

Depending on the location of the finite element on the boundary of the RVE, we distinguish eight cases of calculating the boundary integral occurring in Eq. (2.5). All possible combinations are presented in Table 1. The transition from the system of local coordinates  $\xi, \eta$  to the global system  $x, y$  requires the use of the Jacobian matrix of the transformation

$$(4.1) \quad \mathbf{J} = \begin{bmatrix} \frac{1}{4} [(\eta - 1)x_1 - (\eta - 1)x_2 + (\eta + 1)(x_3 - x_4)] \\ \frac{1}{4} [(\xi - 1)x_1 - (\xi + 1)x_2 + \xi x_3 - \xi x_4 + x_3 + x_4] \\ \frac{1}{4} [(\eta - 1)y_1 - (\eta - 1)y_2 + (\eta + 1)(y_3 - y_4)] \\ \frac{1}{4} [(\xi - 1)y_1 - (\xi + 1)y_2 + \xi y_3 - \xi y_4 + y_3 + y_4] \end{bmatrix},$$

where  $x_i, y_i, i = 1, 2, 3, 4$  are the coordinates of the nodes in the global system of coordinates.

**Table 1.** Cases of integration dependent on the location of the finite element.

Location of the finite element, see Fig. 1	Calculation cases of $\mathbf{C}_u^e$
1	$\mathbf{C}_u^e = \mathbf{C}^{\Gamma_1} = \int_{\Gamma_1} \mathbf{H}_u \mathbf{N}^T \mathbf{N} \cdot \det  \mathbf{J}  d\Gamma_1 = \int_{-1}^1 \mathbf{H}_u \mathbf{N}^T(\xi, -1) \mathbf{N}(\xi, -1) \cdot \det  \mathbf{J}  d\xi$
2	$\mathbf{C}_u^e = \mathbf{C}^{\Gamma_2} = \int_{\Gamma_2} \mathbf{H}_u \mathbf{N}^T \mathbf{N} \cdot \det  \mathbf{J}  d\Gamma_2 = \int_{-1}^1 \mathbf{H}_u \mathbf{N}^T(1, \eta) \mathbf{N}(1, \eta) \cdot \det  \mathbf{J}  d\eta$
3	$\mathbf{C}_u^e = \mathbf{C}^{\Gamma_3} = \int_{\Gamma_3} \mathbf{H}_u \mathbf{N}^T \mathbf{N} \cdot \det  \mathbf{J}  d\Gamma_3 = \int_{-1}^1 \mathbf{H}_u \mathbf{N}^T(\xi, 1) \mathbf{N}(\xi, 1) \cdot \det  \mathbf{J}  d\xi$
4	$\mathbf{C}_u^e = \mathbf{C}^{\Gamma_4} = \int_{\Gamma_4} \mathbf{H}_u \mathbf{N}^T \mathbf{N} \cdot \det  \mathbf{J}  d\Gamma_4 = \int_{-1}^1 \mathbf{H}_u \mathbf{N}^T(-1, \eta) \mathbf{N}(-1, \eta) \cdot \det  \mathbf{J}  d\eta$
12	$\begin{aligned} \mathbf{C}_u^e = \mathbf{C}^{\Gamma_1+\Gamma_2} &= \int_{\Gamma_1} \mathbf{H}_u \mathbf{N}^T \mathbf{N} \cdot \det  \mathbf{J}  d\Gamma_1 + \int_{\Gamma_2} \mathbf{H}_u \mathbf{N}^T \mathbf{N} \cdot \det  \mathbf{J}  d\Gamma_2 \\ &= \int_{-1}^1 \mathbf{H}_u \mathbf{N}^T(\xi, -1) \mathbf{N}(\xi, -1) \cdot \det  \mathbf{J}  d\xi + \int_{-1}^1 \mathbf{H}_u \mathbf{N}^T(1, \eta) \mathbf{N}(1, \eta) \cdot \det  \mathbf{J}  d\eta \end{aligned}$
23	$\begin{aligned} \mathbf{C}_u^e = \mathbf{C}^{\Gamma_2+\Gamma_3} &= \int_{\Gamma_2} \mathbf{H}_u \mathbf{N}^T \mathbf{N} \cdot \det  \mathbf{J}  d\Gamma_2 + \int_{\Gamma_3} \mathbf{H}_u \mathbf{N}^T \mathbf{N} \cdot \det  \mathbf{J}  d\Gamma_3 \\ &= \int_{-1}^1 \mathbf{H}_u \mathbf{N}^T(1, \eta) \mathbf{N}(1, \eta) \cdot \det  \mathbf{J}  d\eta + \int_{-1}^1 \mathbf{H}_u \mathbf{N}^T(\xi, 1) \mathbf{N}(\xi, 1) \cdot \det  \mathbf{J}  d\xi \end{aligned}$
34	$\begin{aligned} \mathbf{C}_u^e = \mathbf{C}^{\Gamma_3+\Gamma_4} &= \int_{\Gamma_3} \mathbf{H}_u \mathbf{N}^T \mathbf{N} \cdot \det  \mathbf{J}  d\Gamma_3 + \int_{\Gamma_4} \mathbf{H}_u \mathbf{N}^T \mathbf{N} \cdot \det  \mathbf{J}  d\Gamma_4 \\ &= \int_{-1}^1 \mathbf{H}_u \mathbf{N}^T(\xi, 1) \mathbf{N}(\xi, 1) \cdot \det  \mathbf{J}  d\xi + \int_{-1}^1 \mathbf{H}_u \mathbf{N}^T(-1, \eta) \mathbf{N}(-1, \eta) \cdot \det  \mathbf{J}  d\eta \end{aligned}$
41	$\begin{aligned} \mathbf{C}_u^e = \mathbf{C}^{\Gamma_4+\Gamma_1} &= \int_{\Gamma_4} \mathbf{H}_u \mathbf{N}^T \mathbf{N} \cdot \det  \mathbf{J}  d\Gamma_4 + \int_{\Gamma_1} \mathbf{H}_u \mathbf{N}^T \mathbf{N} \cdot \det  \mathbf{J}  d\Gamma_1 \\ &= \int_{-1}^1 \mathbf{H}_u \mathbf{N}^T(-1, \eta) \mathbf{N}(-1, \eta) \cdot \det  \mathbf{J}  d\eta + \int_{-1}^1 \mathbf{H}_u \mathbf{N}^T(\xi, -1) \mathbf{N}(\xi, -1) \cdot \det  \mathbf{J}  d\xi \end{aligned}$
0	$\mathbf{C}_u^e = \mathbf{0}$

$$(4.2) \quad \text{Det}[\mathbf{J}] = \frac{1}{8} \{ x_3 [y_1(\xi - \eta) + (\eta + 1)y_4 - (\xi + 1)y_2] \\ + x_2 [-y_4(\eta + \xi) + (\eta - 1)y_1 + (\xi + 1)y_3] - \eta x_1 y_2 + \eta x_1 y_3 - \eta x_4 y_3 \\ - \xi x_4 y_1 + \xi x_4 y_2 - \xi x_1 y_3 + \xi x_1 y_4 + x_4 y_1 + x_1 y_2 - x_4 y_3 - x_1 y_4 \}.$$

An analytical solution to all the integrals included in the table can be found in the paper [2].

## 5. CALCULATION ALGORITHM

On the basis of the publications [4–6, 8–10, 12], we present in Fig. 2 the algorithm of two-scale modelling which was implemented in the author's own software CH\_v\_1.4.2 [2]. This algorithm includes the possibility of non-linearity both at the micro and macro scales.

The fast converging method of conjugate gradients [13] was used to solve the system of FEM equations both at the macro and micro scales. The course of action leading to the solution with this method is presented below. The system of Eqs. (1.2) that defines the finite element form of the boundary value problem at the micro scale is used as an example.

Let us consider the function  $\varphi : \mathbb{R}^N \rightarrow \mathbb{R}$

$$(5.1) \quad \varphi(\mathbf{u}) = \frac{1}{2} \mathbf{u}^T \tilde{\mathbf{K}} \mathbf{u} - \tilde{\mathbf{F}}^T \mathbf{u},$$

where  $\mathbf{u}, \tilde{\mathbf{F}} \in \mathbb{R}^N$  and  $\tilde{\mathbf{K}} = \tilde{\mathbf{K}}^T \in \mathbb{R}^{N \times N}$  is a positively defined symmetric matrix. With these assumptions the function (5.1) has one minimum which is also a global minimum [11]. The extremum is located at the point which satisfies the equation,

$$(5.2) \quad \nabla \varphi = 0.$$

We calculate

$$(5.3) \quad \frac{\partial \varphi}{\partial u_i} = \frac{1}{2} \frac{\partial}{\partial u_i} \sum_{j,k} \tilde{K}_{jk} u_j u_k - \frac{\partial}{\partial u_i} \sum_j \tilde{F}_j u_j \\ = \frac{1}{2} \sum_{j,k} \tilde{K}_{jk} \left( \frac{\partial u_j}{\partial u_i} u_k + u_j \frac{\partial u_k}{\partial u_i} \right) - \sum_j \tilde{F}_j \frac{\partial u_j}{\partial u_i} \\ = \frac{1}{2} \sum_{j,k} \tilde{K}_{jk} (\delta_{ij} u_k + u_j \delta_{ik}) - \sum_j \tilde{F}_j \delta_{ij} = \frac{1}{2} \sum_k \tilde{K}_{ik} u_k + \frac{1}{2} \sum_j \tilde{K}_{ji} u_j - \tilde{F}_i \\ = \frac{1}{2} \sum_k \tilde{K}_{ik} u_k + \frac{1}{2} \sum_j \tilde{K}_{ij} u_j - \tilde{F}_i = \left( \tilde{\mathbf{K}} \mathbf{u} - \tilde{\mathbf{F}} \right)_i.$$

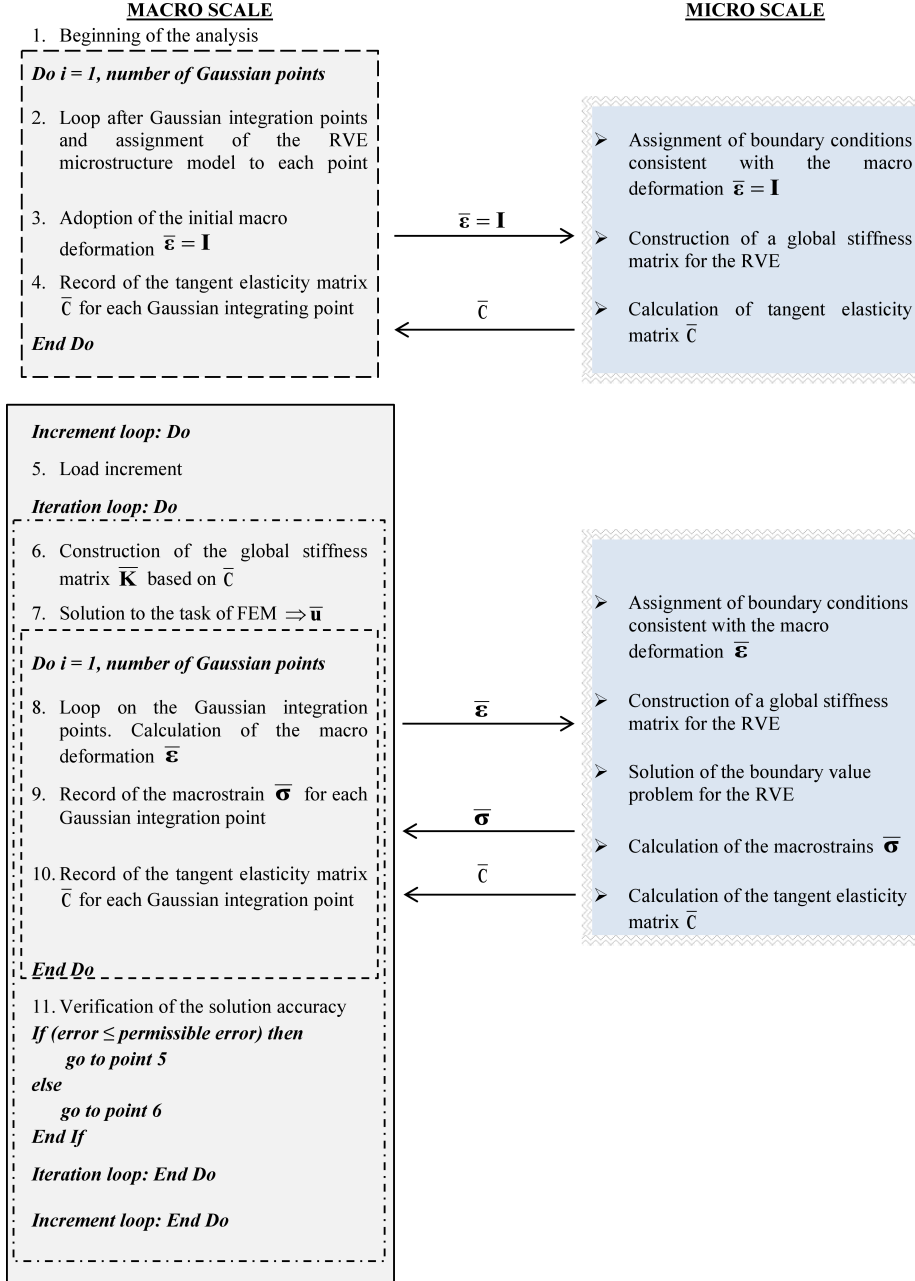


FIG. 2. An algorithm of two-scale modelling (numerical homogenization).

The function (5.1) reaches a minimum when

$$(5.4) \quad \tilde{\mathbf{K}} \mathbf{u} - \tilde{\mathbf{F}} = \mathbf{0} \Leftrightarrow \tilde{\mathbf{K}} \mathbf{u} = \tilde{\mathbf{F}}.$$

Therefore, the solution to the above system of equations boils down to finding a minimum of the positively defined square form (5.1). The solution with the conjugate gradient method will proceed according to the following algorithm:

$$\begin{array}{l}
 \mathbf{r}_1 = \tilde{\mathbf{F}} - \tilde{\mathbf{K}} \mathbf{u}_1, \quad \mathbf{p}_1 = \mathbf{r}_1 \\
 \text{do while } \|\mathbf{r}_k\| > \delta \\
 \alpha_k = \frac{\mathbf{r}_k^T \mathbf{r}_k}{\mathbf{p}_k^T \tilde{\mathbf{K}} \mathbf{p}_k} \\
 \mathbf{r}_{k+1} = \mathbf{r}_k - \alpha_k \tilde{\mathbf{K}} \mathbf{p}_k \\
 \beta_k = \frac{\mathbf{r}_{k+1}^T \mathbf{r}_{k+1}}{\mathbf{r}_k^T \mathbf{r}_k} \\
 \mathbf{p}_{k+1} = \mathbf{r}_{k+1} + \beta_k \mathbf{p}_k \\
 \mathbf{u}_{k+1} = \mathbf{u}_k + \alpha_k \mathbf{p}_k \\
 \text{end do}
 \end{array}$$

where  $\mathbf{u}_1$  is the initial solution and  $0 < \delta \ll 1$ .

## 6. NUMERICAL SIMULATIONS

In order to check whether the two-scale algorithm works properly, a test was run for an isotopic material with a homogenous microstructure described in micro scale with a linearly elastic dependence. The calculations were carried out for a plane state of stress. In this case a two-scale analysis should generate the elasticity matrix  $\mathbf{D}^t$  in the form

$$(6.1) \quad \mathbf{D}^t = \begin{bmatrix} \frac{E}{1-\nu^2} & \frac{E\nu}{1-\nu^2} & 0 \\ \frac{E\nu}{1-\nu^2} & \frac{E}{1-\nu^2} & 0 \\ 0 & 0 & \frac{E}{2(1+\nu)} \end{bmatrix},$$

where the index  $t$  stands for a theoretical (expected) value,  $E$  and  $\nu$  denote the material parameters of the microstructure. In order to check whether the calculations carried out with the own home-made software were correct, they were compared with the results obtained with the professional Abaqus software.

The test was run for a 0.1 m thick disk with the dimensions, type of load, supports and microstructure parameters as in Fig. 3. The elements of the elasticity matrix (6.1) at the macro level should have the following values

$$(6.2) \quad \mathbf{D}^t = \begin{bmatrix} 29761.90 & 4761.90 & 0 \\ 4761.90 & 29761.90 & 0 \\ 0 & 0 & 12500.00 \end{bmatrix}.$$

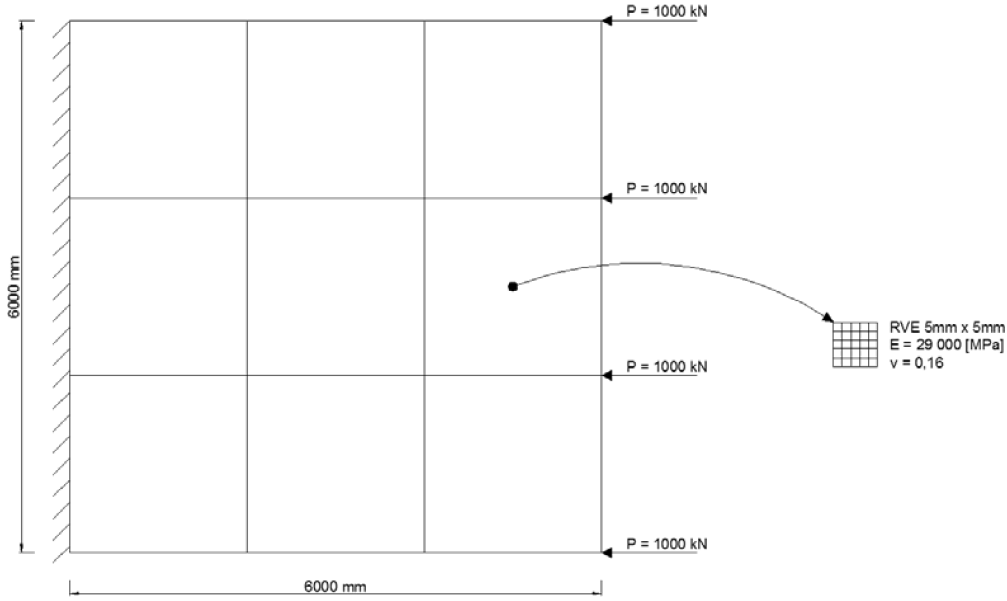


FIG. 3. Disk in the plane state stress, the material microstructure modelled with a homogeneous RVE.

On the macro level the following elasticity matrix values (6.3) were obtained from the two-scale analysis, with the values of homogenized material parameters at the macro level  $\bar{E} = 28999.71$  MPa,  $\bar{\nu} = 0.16$ ,  $\bar{G} = 12499.88$  MPa. In comparison with the expected values (6.2) the obtained results give a relative error of  $\delta = 0.000979\%$ , each element of the matrix (6.3) is determined with the same precision

$$(6.3) \quad \mathbf{D}^{CH} = \begin{bmatrix} 29761.61 & 4761.86 & 0 \\ 4761.86 & 29761.61 & 0 \\ 0 & 0 & 12499.88 \end{bmatrix}.$$

Table 2. Macro stresses.

Element No.	$\bar{\sigma}_{11}^{CH}$ [MPa]	$\bar{\sigma}_{11}$ [MPa]	$\delta$ [%]	$\bar{\sigma}_{22}^{CH}$ [MPa]	$\bar{\sigma}_{22}$ [MPa]	$\delta$ [%]	$\bar{\sigma}_{12}^{CH}$ [MPa]	$\bar{\sigma}_{12}$ [MPa]	$\delta$ [%]
1	-0.006504	-0.006506	0.03	-0.000535	-0.000537	0.43	-0.000413	-0.000411	0.39
2	-0.007099	-0.007098	0.02	-0.000886	-0.000881	0.51	0.001008	0.001006	0.16
3	-0.009053	-0.009045	0.09	0.000947	0.000944	0.27	0.000947	0.000947	0.04
4	-0.006992	-0.006989	0.04	-0.001069	-0.001068	0.14	0.000000	0.000000	0.00
5	-0.005802	-0.005803	0.02	-0.001771	-0.001767	0.23	0.000000	0.000000	0.00
6	-0.001893	-0.001909	0.83	0.001893	0.001890	0.17	0.000000	0.000000	0.00
7	-0.006504	-0.006506	0.03	-0.000535	-0.000537	0.43	0.000413	0.000411	0.39
8	-0.007099	-0.007098	0.02	-0.000886	-0.000881	0.51	-0.001008	-0.001006	0.16
9	-0.009053	-0.009045	0.09	0.000947	0.000944	0.27	-0.000947	-0.000947	0.04

Table 3. Macro deformations.

Element No.	$\bar{\varepsilon}_{11}^{CH}$	$\varepsilon_{11}$	$\delta$ [%]	$\bar{\varepsilon}_{22}^{CH}$	$\varepsilon_{22}$	$\delta$ [%]	$\bar{\varepsilon}_{12}^{CH}$	$\varepsilon_{12}$	$\delta$ [%]
1	-2.213E-07	-2.214E-07	0.05	1.740E-08	1.738E-08	0.12	-3.300E-08	-3.287E-08	0.40
2	-2.399E-07	-2.399E-07	0.00	8.600E-09	8.774E-09	1.98	8.060E-08	8.047E-08	0.16
3	-3.174E-07	-3.171E-07	0.09	8.260E-08	8.246E-08	0.17	7.570E-08	7.577E-08	0.09
4	-2.352E-07	-2.351E-07	0.04	1.700E-09	1.749E-09	2.80	0.000E+00	8.747E-23	0.00
5	-1.903E-07	-1.904E-07	0.05	-2.910E-08	-2.892E-08	0.62	0.000E+00	5.811E-23	0.00
6	-7.570E-08	-7.626E-08	0.73	7.570E-08	7.570E-08	0.00	0.000E+00	-3.640E-23	0.00
7	-2.213E-07	-2.214E-07	0.05	1.740E-08	1.738E-08	0.12	3.300E-08	3.287E-08	0.40
8	-2.399E-07	-2.399E-07	0.00	8.600E-09	8.774E-09	1.98	-8.060E-08	-8.047E-08	0.16
9	-3.174E-07	-3.171E-07	0.09	8.260E-08	8.246E-08	0.17	-7.570E-08	-7.577E-08	0.09

In order to verify the calculations, the results for macro stresses, macro deformations and macro displacements were compared. In the tables below the following denotations have been adopted:  $\bar{\sigma}_{11}^{CH}$ ,  $\bar{\varepsilon}_{11}^{CH}$ ,  $\bar{u}^{CH}$ ,  $\bar{v}^{CH}$  – respectively the components of the state of macro stress, macro deformation, horizontal and vertical displacements of FE nodes, determined with the two-scale algorithm. We have used a 4-node 8-dof rectangular finite element with bilinear shape functions. The values without the upper index  $^{CH}$  were calculated with the Abaqus software, using the finite element CPS4R (a 4-node bilinear plane stress quadrilateral, reduced integration, hourglass control).

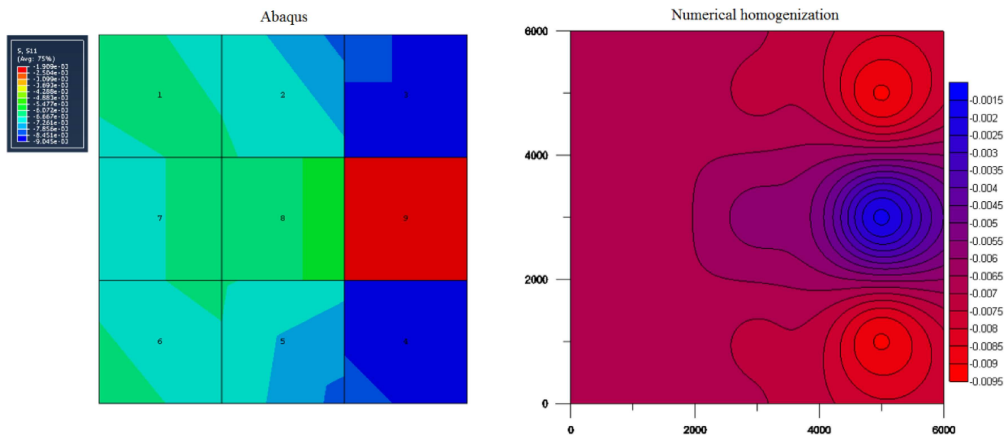


FIG. 4. Field of macro stresses: Abaqus  $\bar{\sigma}_{11}$ , numerical homogenization  $\bar{\sigma}_{11}^{CH}$ .

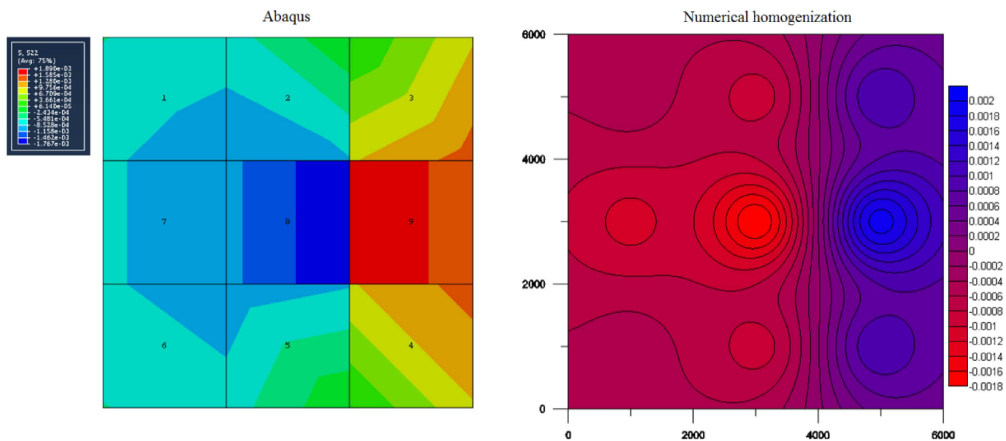


FIG. 5. Field of macro stresses: Abaqus  $\bar{\sigma}_{22}$ , numerical homogenization  $\bar{\sigma}_{22}^{CH}$ .

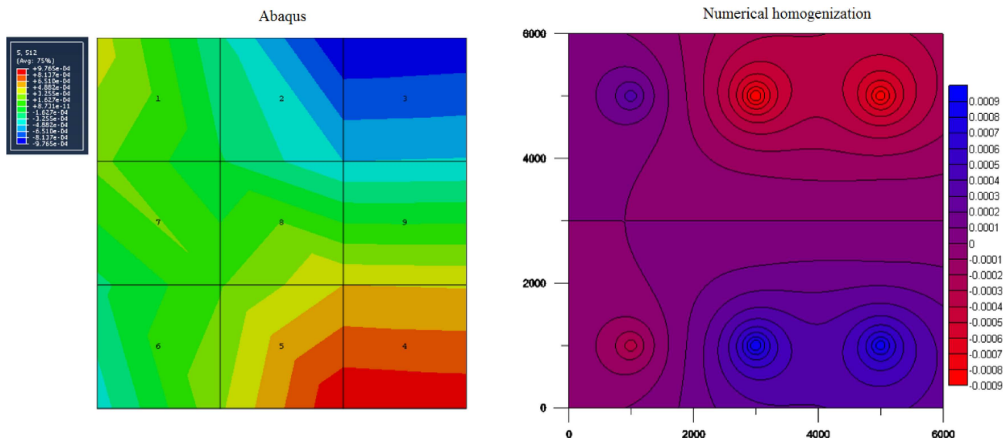


FIG. 6. Field of macro stresses: Abaqus  $\bar{\sigma}_{12}$ , numerical homogenization  $\bar{\sigma}_{12}^{CH}$ .

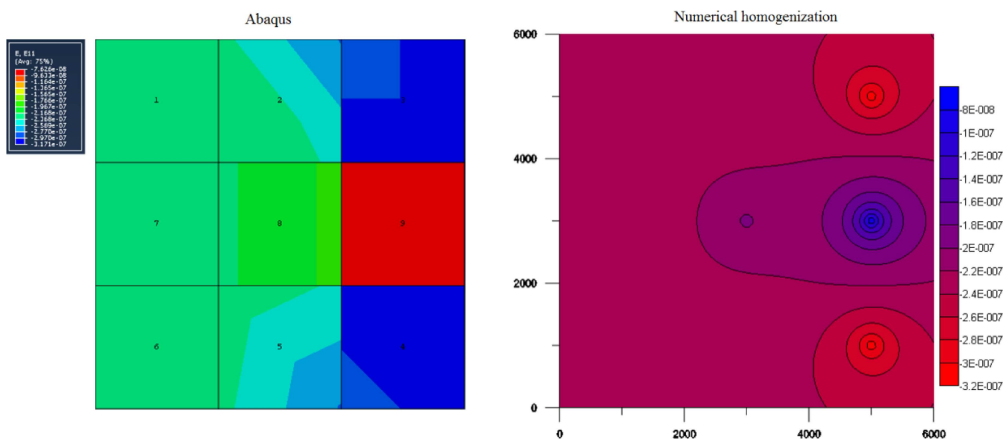


FIG. 7. Field of macro strains: Abaqus  $\bar{\epsilon}_{11}$ , numerical homogenization  $\bar{\epsilon}_{11}^{CH}$ .

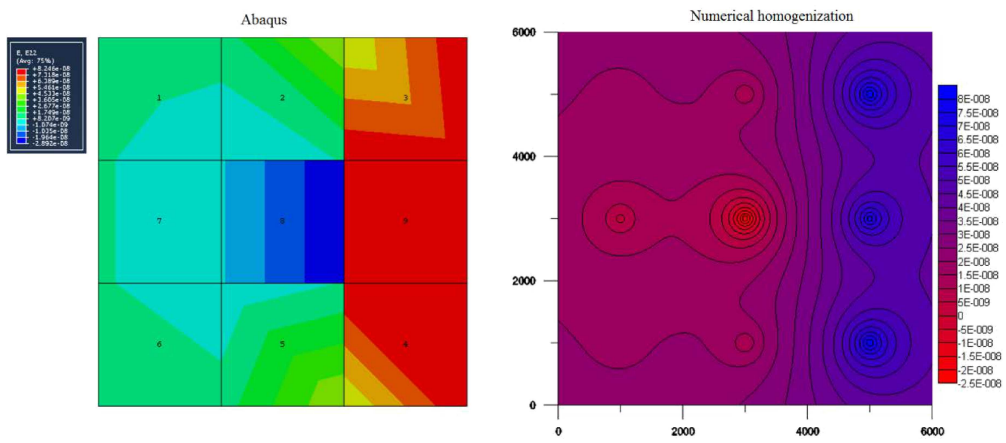


FIG. 8. Field of macro strains: Abaqus  $\bar{\epsilon}_{22}$ , numerical homogenization  $\bar{\epsilon}_{22}^{CH}$ .

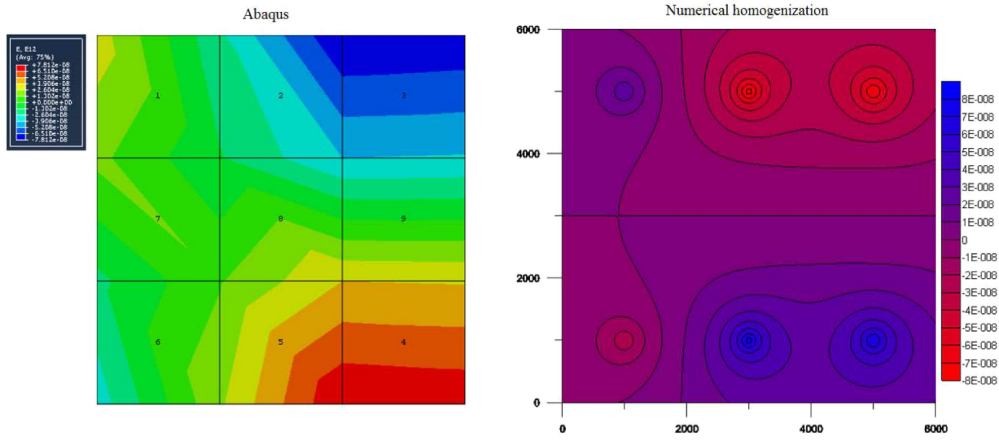


FIG. 9. Field of macro strains: Abaqus  $\bar{\varepsilon}_{12}$ , numerical homogenization  $\bar{\varepsilon}_{12}^{CH}$ .

**Table 4.** Macro displacements.

Node No.	$\bar{u}^{CH}$ [m]	$\bar{u}$ [m]	$\delta$ [%]	$\bar{v}^{CH}$ [m]	$\bar{v}$ [m]	$\delta$ [%]
1	0.000E+00	-6.916E-37	0.00	0.000E+00	-9.483E-38	0.00
2	-4.149E-04	-4.152E-04	0.08	-7.318E-05	-7.302E-05	0.22
3	-9.940E-04	-9.942E-04	0.02	9.678E-05	9.576E-05	1.06
4	-2.112E-03	-2.110E-03	0.10	-5.786E-04	-5.770E-04	0.28
5	0.000E+00	-1.308E-36	0.00	0.000E+00	-9.411E-38	0.00
6	-4.704E-04	-4.702E-04	0.04	-3.396E-06	-3.498E-06	3.02
7	-8.510E-04	-8.509E-04	0.00	6.152E-05	6.133E-05	0.31
8	-1.002E-03	-1.003E-03	0.10	-2.130E-04	-2.127E-04	0.11
9	0.000E+00	-1.308E-36	0.00	0.000E+00	9.411E-38	0.00
10	-4.704E-04	-4.702E-04	0.04	3.396E-06	3.498E-06	3.02
11	-8.510E-04	-8.509E-04	0.00	-6.152E-05	-6.133E-05	0.31
12	-1.002E-03	-1.003E-03	0.10	2.130E-04	2.127E-04	0.11
13	0.000E+00	-6.916E-37	0.00	0.000E+00	9.483E-38	0.00
14	-4.149E-04	-4.152E-04	0.08	7.318E-05	7.302E-05	0.22
15	-9.940E-04	-9.942E-04	0.02	-9.678E-05	-9.576E-05	1.06
16	-2.112E-03	-2.110E-03	0.10	5.786E-04	5.770E-04	0.28

Further analyses were directed at obtaining effective material parameters of reactive powder concrete at the macro level by two-scale modelling with the use of the microstructure model described in [2, 3]. First, ten random RVEs were generated (Fig. 13) with the following composition:

- Red colour represents the cement matrix – quantitative participation 47.08%,
- Light blue colour represents thicker aggregate – quantitative participation 40.52%,
- Dark blue colour represents finer aggregate – quantitative participation 8.40%,
- Yellow colour represents pores (air voids) – quantitative participation 4%.

The material parameters adopted for the analysis were:

- Cement matrix  $E = 29000$  MPa,  $\nu = 0.2$ ,
- Thick aggregate  $E = 75000$  MPa,  $\nu = 0.3$ ,
- Fine aggregate  $E = 55000$  MPa,  $\nu = 0.3$ ,
- pores (air voids) – empty space without finite elements.

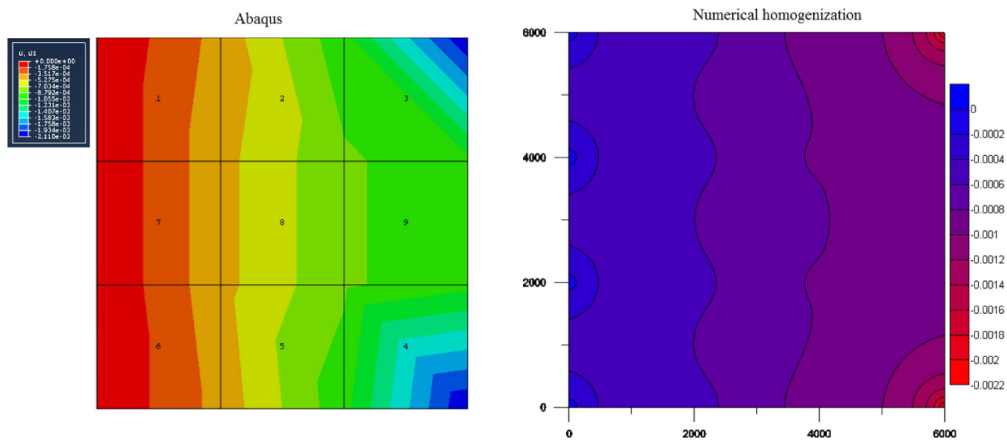


FIG. 10. Field of horizontal macro displacements: Abaqus  $\bar{u}$ , numerical homogenization  $\bar{u}^{CH}$ .

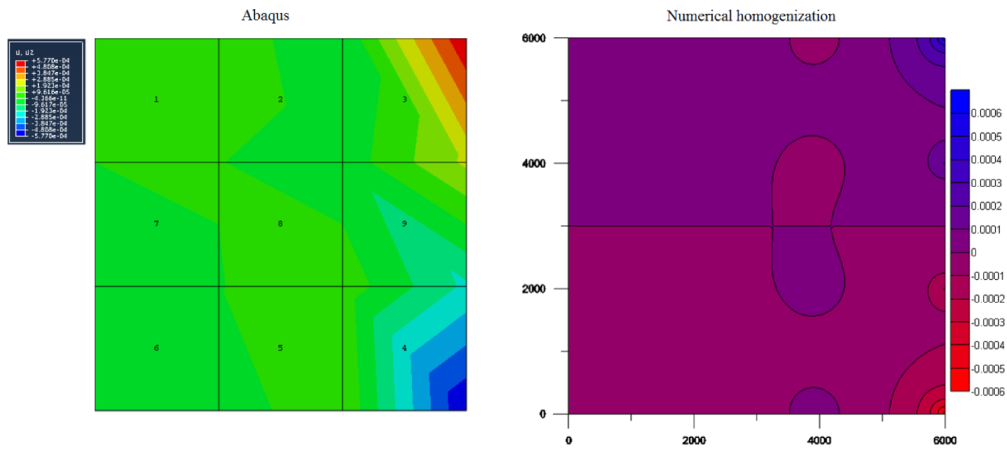


FIG. 11. Field of vertical macro displacements: Abaqus  $\bar{v}$ , numerical homogenization  $\bar{v}^{CH}$ .

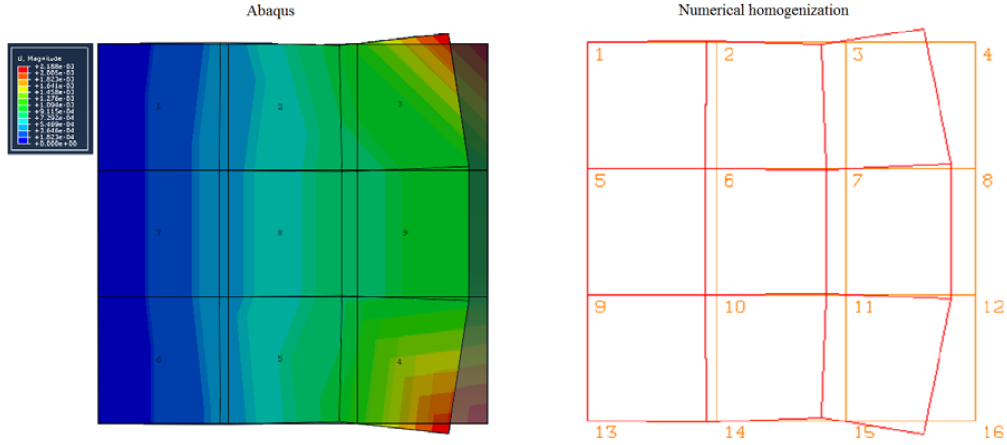


FIG. 12. Form of the disk deformation at the macro scale.

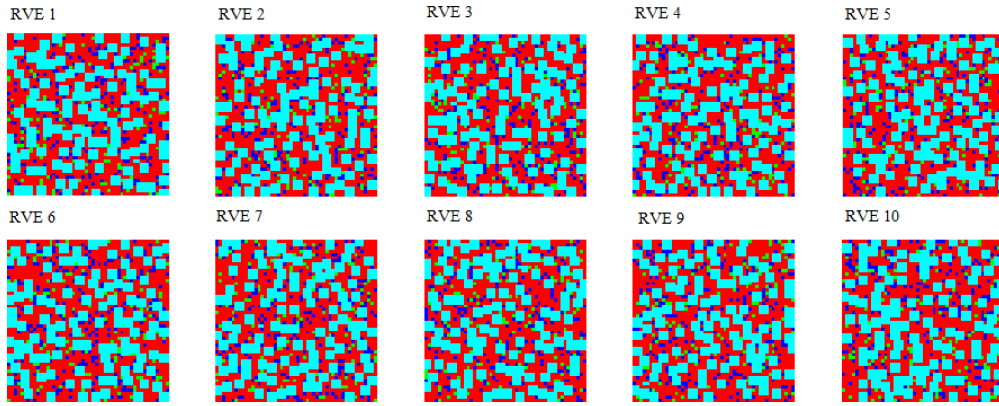


FIG. 13. Randomly generated RVEs.

The main and only goal of this task was to determine effective material parameters on the macro level, i.e. the task was not solved for macro scale (the first block of the algorithm presented in Fig. 2 was done). The state of macro deformation corresponding to pure shearing  $\bar{\boldsymbol{\varepsilon}} = \{0, 0, 1\}$  was adopted for the analysis. The macro stresses  $\bar{\boldsymbol{\sigma}}$  and the macro elasticity matrix  $\bar{\mathbf{C}}$  were determined. Using the constitutive relation for an isotropic linearly elastic material the macro deformations were calculated from the relationship

$$(6.4) \quad \bar{\boldsymbol{\varepsilon}} = \bar{\mathbf{C}}^{-1} \bar{\boldsymbol{\sigma}}.$$

The results are presented in Tables 5–7 and in Fig. 14. In addition, the expected (mean) values of macro parameters were calculated

$$(6.5) \quad x^{sr} = \frac{1}{10} \sum_{i=1}^{10} x_i,$$

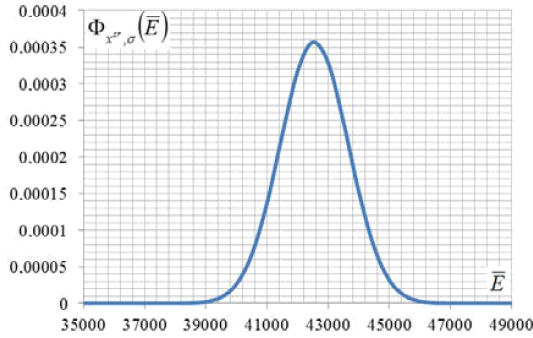
where  $x$  denotes the value of Young's modulus, Poisson's ratio and the shear modulus (Kirchhoff's modulus) The standard deviation for each parameter

$$(6.6) \quad \sigma = \sqrt{\sigma^2} \quad \text{where} \quad \sigma^2 = \frac{1}{9} \sum_{i=1}^{10} (x_i - x^{sr})^2$$

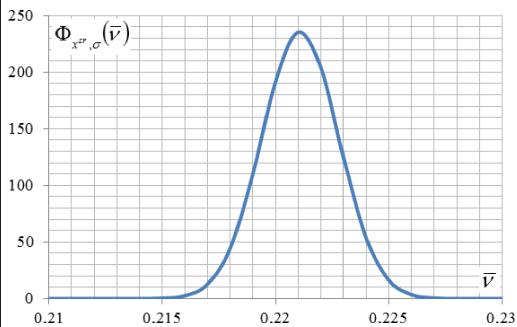
and the normal distribution density function was determined

$$(6.7) \quad \Phi_{x^{sr}, \sigma}(x) = \frac{1}{\sigma\sqrt{2\pi}} \exp\left(\frac{-(x - x^{sr})^2}{2\sigma^2}\right).$$

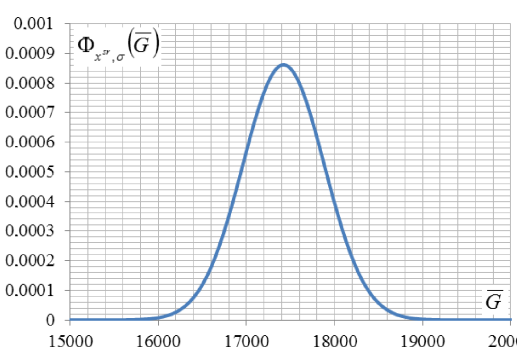
**Table 5.** Elasticity modulus.

RVE No.	$\bar{E}$ [MPa]	Standard deviation	Expected value	Normal distribution density function
1	43421.50	1116.66	42545.52	
2	43440.90			
3	42052.52			
4	41084.63			
5	44356.80			
6	42572.80			
7	42954.21			
8	40679.34			
9	42849.57			
10	42042.97			

**Table 6.** Poisson's ratio.

RVE No.	$\bar{\nu}$	Standard deviation	Expected value	Normal distribution density function
1	0.2219	0.0017	0.2211	
2	0.2207			
3	0.2205			
4	0.2203			
5	0.2213			
6	0.2201			
7	0.2203			
8	0.2251			
9	0.2220			
10	0.2188			

**Table 7.** The shear modulus.

RVE No.	$\bar{G}$ [MPa]	Standard deviation	Expected value	Normal distribution density function
1	17767.60	463.26	17421.28	
2	17793.70			
3	17228.22			
4	16833.99			
5	18159.84			
6	17446.77			
7	17600.39			
8	16602.70			
9	17531.91			
10	17247.71			

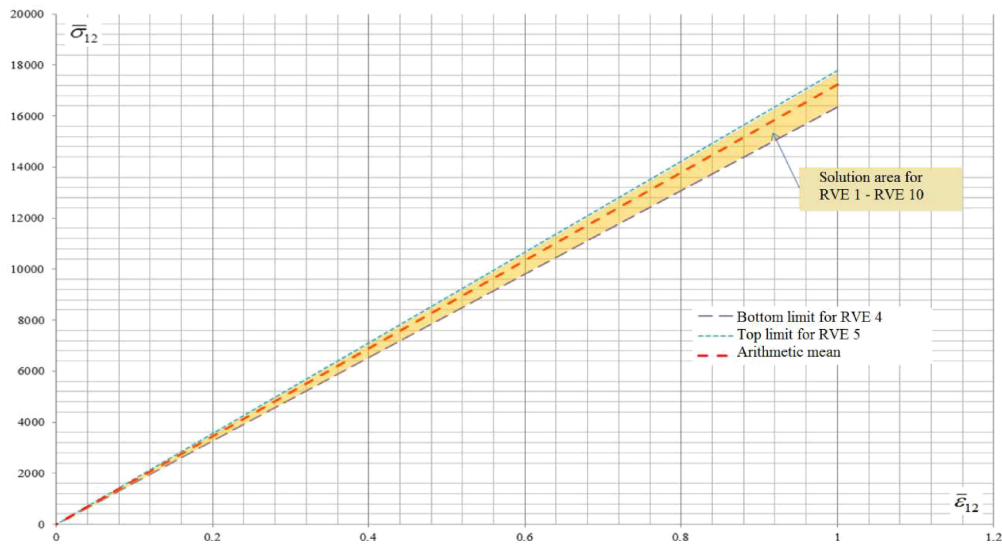


FIG. 14. The stress-deformation dependence for pure shearing at the macro scale.

For the sake of clarity all straight lines showing the linear stress-strain relationship have been removed from the above diagram except for the two that correspond to the cells RVE 4 and RVE 5, which are respectively lower and upper limits of the obtained results. The averaged relationship from all the RVEs is also presented.

## 7. CONCLUSIONS

The paper presents a method of two-scale modelling for determining effective material parameters of reactive powder concrete at the macro scale on the basis

of the analysis of its microstructure in the range of linear elasticity. The displacement version of the finite element method was used to solve the boundary value problems at both scales. The problems were analysed for a plane state of stress. At the macro level (construction) and at the micro level (material microstructure) a four-node rectangular finite element with two nodal degrees of freedom was used. The displacement field within the element was approximated with bilinear shape functions [3, 2].

The method of two-scale modelling makes it necessary to enforce deformation on the boundary of a representative volume element (RVE) consistent with the adopted or calculated macro deformation. The paper presents the realisation of this task through aggregation of the RVE global stiffness matrix with analytically calculated (without numerical integration) matrices  $\mathbf{C}_u^e$ , whose form depends on the location of the aggregated finite element in relation to the RVE boundary.

The results of numerical examples presented in this paper confirm that the authors' own software CH\_v\_1.4.2, in which the two-scale model of reactive powder concrete is implemented, works properly. The solutions to the boundary value problems of mechanics for the RVE (micro analysis) [3, 2] and the full two-scale modelling (micro-macro) bring expected results and are consistent with publications by other researchers.

A complex comparison of the results of numerical simulations for beams and the results of experimental tests in terms of determination of constitutive material parameters will be the subject of the third part of this series.

#### REFERENCES

1. AINSWORTH M., *Essential boundary conditions and multi-point constraints in finite element analysis*, Computer Methods in Applied Mechanics and Engineering, **190**, 6323–6339, 2001.
2. DENISIEWICZ A., *Modelowanie dwuskalowe związków konstytutywnych betonu z proszków reaktywnych i ich walidacja doświadczalna* [in Polish], PhD thesis, Supervisor prof. M. Kuczma, University of Zielona Góra, 2013.
3. DENISIEWICZ A., KUCZMA M., *Two-scale modelling of reactive powder concrete. Part I: representative volume element and solution of the corresponding boundary value problem*, Civil and Environmental Engineering Reports, **10**, 41–61, 2013.
4. FEYEL F., *A multilevel finite element method FE2 to describe the response of highly nonlinear structures using generalized continua*, Computer Methods in Applied Mechanics and Engineering, **192**, 3233–3244, 2003.
5. FEYEL F., *Multiscale FE2 elastoviscoplastic analysis of composite structures*, Computational Materials Science, **16**, 344–354, 1999.

6. GHOSH S., LEE K., MOORTHY S., *Two scale analysis of heterogeneous elastic-plastic materials with asymptotic homogenization and Voronoi cell finite element model*, Computer Methods in Applied Mechanics and Engineering, **132**, 63–116, 1996.
7. KACZMARCZYK Ł., *Numeryczna analiza wybranych problemów mechaniki ośrodków niejednorodnych* [in Polish], PhD thesis, Cracow University of Technology, 2006.
8. KACZMARCZYK Ł., PARCE CH. J., BIĆANIĆ N., *Scale transition and enforcement of RVE boundary conditions in second-order computational homogenization*, Int. J. Numer. Meth. Engng., **74**, 506–522, 2008.
9. KOUZNETSOVA V.G., *Computational homogenization for the multi-scale analysis of multi-phase materials*, Technische Universiteit, Eindhoven, 2002.
10. KOUZNETSOVA V.G., GEERS M.G.D., BREKELMANS W.A.M., *Multi-scale second-order computational homogenization of multi-phase materials: a nested finite element solution strategy*, Computer Methods in Applied Mechanics and Engineering, **193**, 5525–5550, 2004.
11. KUCZMA M., *Podstawy mechaniki konstrukcji z pamięcią kształtu. Modelowanie i numeryka* [in Polish], Publishing house University of Zielona Gora, 2010.
12. MIEHE C., *Computational micro-to-macro transitions for discretized microstructures of heterogeneous materials at finite strains based on the minimization of averaged incremental energy*, Computer Methods in Applied Mechanics and Engineering, **192**, 559–591, 2003.
13. VAN DER VORST H.A., *Linear Algebraic Solvers and Eigenvalue Analysis*, [in:] Encyclopedia of Computational Mechanics, vol. 1: Fundamentals, E. Stein, R.D. Borst, T.J.R. Hughes [Eds.], J. Wiley and Sons, Chichester, 551–576, 2004.